appear to be at least partially intrinsic, because these differences were maintained outside their normal niche. When cells from E13.5 *Cux2-Cre;Ai9* embryos were cultured in vitro at clonal density (Fig. 3C), the majority of $Cux2^+$ progenitors divided symmetrically to generate pairs of RGCs, whereas $Cux2^-$ progenitors preferentially underwent neurogenic divisions (Fig. 3D). We conclude that at early stages of corticogenesis, $Cux2^+$ RGCs fated to generate upper-layer neurons preferentially proliferate to enlarge the precursor pool, whereas $Cux2^-$ RGCs already generate lower-layer neurons.

We next asked whether the generation of distinct neuronal subtypes is an intrinsic property of the two different progenitor types. Dissociated cortical cells from *Cux2-Cre;Ai9* embryos were cultured until they differentiated and were stained with layer-specific markers (Fig. 4, A and C). The in vivo situation was recapitulated in vitro, with ~80% of the $Cux2^+$ progenitors generating neurons with upper-layer identity (Fig. 4B) and the majority of the $Cux2^-$ progenitors producing neurons with lower-layer identity (Fig. 4D). Thus, the neurogenic differences between the two progenitor populations are maintained outside their normal developmental niche, indicating an intrinsic aspect to their divergent fate specification. This result also suggests that birthdate may not be causative to cell fate. To test this hypothesis, we electroporated dominant-negative TCF4 into $Cux2^+$ RGCs to force their premature cell cycle exit (*19*), so that they generated neurons at the expense of self-renewal (fig. S5). These prematurely generated $Cux2^+$ neurons still preferentially occupied upper layers (Fig. 4, E and F) and expressed upper-layer, but not lower-layer, markers (Fig. 4, G to I), indicating that their fate was not altered by the change in birthdate. Thus, $Cux2^+$ RGCs are intrinsically specified to generate upper-layer neurons, independent of niche or birthdate.

Our data show that a subset of RGCs is specified to generate upper-layer neurons regardless of birthdate, but these progenitors are intrinsically programmed to generate neurons predominantly later than their lower-layer counterparts. Thus, contrary to the prevailing model (*2*), our study indicates that molecular fate specification ensures proper birth order, rather than vice versa. Our data also suggest that the minor fraction of callosal projection neurons found in lower layers is derived from the same RGC pool as the major population of callosal neurons in upper layers, demonstrating a common lineage for these functionally similar neurons, irrespective of cortical layer position. Although this model applies to the broad RGC subclasses that generate intracortical versus subcortical/subcerebral projection neurons, it remains possible that the potential of $Cux2^+$ and $Cux2^-$ progenitors is subsequently progressively restricted to further specify neuronal subtypes within the two lineages.

Upper cortical layers are expanded in primates and are required for high-level associative connectivity. Defects in their function are implicated in the etiology of cognitive syndromes such as schizophrenia and autism. The subventricular zone of primates, and especially humans, is enlarged compared with other species and contains outer subventricular RGCs that are thought to generate increased numbers of upper-layer cortical neurons in the primate brain (*20*). Our findings suggest that an equally important evolutionary advance was the subdivision of labor among RGCs in the ventricular zone to generate lower- and upper-layer neurons.

References and Notes

1. B. J. Molyneaux, P. Arlotta, J. R. L. Menezes, J. D. Macklis, *Nat. Rev. Neurosci.* **8**, 427 (2007).
2. D. P. Leone, K. Srinivasan, B. Chen, E. Alcamo, S. K. McConnell, *Curr. Opin. Neurobiol.* **18**, 28 (2008).
3. R. F. Hevner *et al.*, *Dev. Neurosci.* **25**, 139 (2003).
4. T. Kowalczyk *et al.*, *Cereb. Cortex* **19**, 2439 (2009).
5. M. Nieto *et al.*, *J. Comp. Neurol.* **479**, 168 (2004).
6. C. Zimmer, M.-C. Tiveron, R. Bodmer, H. Cremer, *Cereb. Cortex* **14**, 1408 (2004).
7. S. J. Franco, I. Martinez-Garay, C. Gil-Sanz, S. R. Harkins-Perry, U. Müller, *Neuron* **69**, 482 (2011).
8. E. A. Alcamo *et al.*, *Neuron* **57**, 364 (2008).
9. O. Britanova *et al.*, *Neuron* **57**, 378 (2008).
10. F. Schnütgen *et al.*, *Nat. Biotechnol.* **21**, 562 (2003).
11. R. Feil, J. Wagner, D. Metzger, P. Chambon, *Biochem. Biophys. Res. Commun.* **237**, 752 (1997).
12. S. Hayashi, A. P. McMahon, *Dev. Biol.* **244**, 305 (2002).
13. M. Zervas, S. Millet, S. Ahn, A. L. Joyner, *Neuron* **43**, 345 (2004).
14. F. Balordi, G. Fishell, *J. Neurosci.* **27**, 14248 (2007).
15. M. R. Costa, O. Bucholz, T. Schroeder, M. Götz, *Cereb. Cortex* **19** (suppl. 1), i135 (2009).
16. T. Takahashi, T. Goto, S. Miyama, R. S. Nowakowski, V. S. Caviness Jr., *J. Neurosci.* **19**, 10357 (1999).
17. K.-I. Mizutani, K. Yoon, L. Dang, A. Tokunaga, N. Gaiano, *Nature* **449**, 351 (2007).
18. K.-J. Yoon *et al.*, *Neuron* **58**, 519 (2008).
19. G. J. Woodhead, C. A. Mutch, E. C. Olson, A. Chenn, *J. Neurosci.* **26**, 12620 (2006).
20. J. H. Lui, D. V. Hansen, A. R. Kriegstein, *Cell* **146**, 18 (2011).

Acknowledgments: We thank G. Fishell for *Nestin-CreERT2* mice; H. Zeng for *Ai9* reporter mice; P. Chambon for *pCreERT2*; A. Maximov for the FLEx backbone; T. Wagner, S. Courtes, and P. Kazmierczak for experiments that did not appear in the final manuscript; and F. Polleux, E. Grove, N. Grillet, and S. Courtes for critical comments. This work was supported by the NIH (S.J.F., NS060355; U.M., NS046456 and MH078833), Generalitat Valenciana (C.G.-S., APOSTD/2010/064), Ministerio de Educacion (C.G.-S., EX2009-0416; I.M.-G., FU-2006-1238), CIRM training grant (I.M.-G. and A.E.), the Skaggs Institute for Chemical Biology (U.M.), and the Dorris Neuroscience Center (U.M.). S.J.F., I.M.-G., C.G.-S., and U.M. conceived the project; S.J.F., C.G.-S., I.M.-G., and A.E. designed, performed, and analyzed experiments with assistance from S.R.H.-P. and C.R.; and S.J.F. and U.M. prepared the manuscript, with revisions from C.G.-S., I.M.-G., and A.E.

Supplementary Materials

www.sciencemag.org/cgi/content/full/337/6095/746/DC1
Materials and Methods
Figs. S1 to S5
References (*21*–*29*)

20 April 2012; accepted 14 June 2012
10.1126/science.1223616

Bergmann Glial AMPA Receptors Are Required for Fine Motor Coordination

Aiman S. Saab,[1,2] Alexander Neumeyer,[3]* Hannah M. Jahn,[1,2]*† Alexander Cupido,[1]* Antonia A. M. Šimek,[4]* Henk-Jan Boele,[4] Anja Scheller,[1,2] Karim Le Meur,[1]‡ Magdalena Götz,[5,6] Hannah Monyer,[7] Rolf Sprengel,[8] Maria E. Rubio,[9] Joachim W. Deitmer,[3] Chris I. De Zeeuw,[4,10]§ Frank Kirchhoff[1,2]§

The impact of glial neurotransmitter receptors in vivo is still elusive. In the cerebellum, Bergmann glial (BG) cells express α-amino-3-hydroxy-5-methyl-4-isoxazolepropionic acid (AMPA)–type glutamate receptors (AMPARs) composed exclusively of GluA1 and/or GluA4 subunits. With the use of conditional gene inactivation, we found that the majority of cerebellar GluA1/A4-type AMPARs are expressed in BG cells. In young mice, deletion of BG AMPARs resulted in retraction of glial appendages from Purkinje cell (PC) synapses, increased amplitude and duration of evoked PC currents, and a delayed formation of glutamatergic synapses. In adult mice, AMPAR inactivation also caused retraction of glial processes. The physiological and structural changes were accompanied by behavioral impairments in fine motor coordination. Thus, BG AMPARs are essential to optimize synaptic integration and cerebellar output function throughout life.

Astroglial cells sense synaptic activity through various neurotransmitter receptors and are considered to modulate neuronal processing (*1*–*3*). In the cerebellar cortex, ectopic release of glutamate from climbing and parallel fiber terminals activates Ca^{2+}-permeable α-amino-3-hydroxy-5-methyl-4-isoxazolepropionic acid (AMPA)–type glutamate receptors (AMPARs) expressed on Bergmann glial (BG) appendages (*4*) that tightly enwrap Purkinje cell (PC) synapses (*5*). Conversion of BG AMPARs into Ca^{2+}-impermeable receptors by adenoviral-mediated delivery of the GluA2 gene (*6*) caused BG process retraction from PC synapses and altered PC excitatory postsynaptic currents (EPSCs), providing insight into the functional interaction between BG and glutamatergic synapses. However, whether BG AMPAR signaling influences cerebellar function in vivo has remained unknown.

To investigate the impact of BG AMPARs on cerebellar function, we generated inducible double knockouts (dKOs) to ablate GluA1 and GluA4 (*Gria1* and *Gria4*) AMPAR subunits selectively in astrocytes in a temporally controlled fashion. We crossed mice expressing the tamoxifen-sensitive Cre-recombinase CreERT2 under the astrocyte-specific, endogenous GLAST (Slc1a3)-promoter (*7*) with mice carrying loxP-flanked *Gria1* (*8*) and *Gria4* (*9*) alleles (Fig. 1A). Because BG cells express only the AMPAR subunits GluA1 and GluA4 (*10*, *11*), inactivation of both subunits will result in a complete loss of AMPAR function.

We injected mice (GLAST$^{CreERT2/+}$ × Gria1$^{fl/fl}$ × Gria4$^{fl/fl}$, termed dKO) with tamoxifen at postnatal day 14 (P14) for 5 days and studied BG AMPAR ablation 10 to 14 days after treatment (Fig. 1A). Control mice were homozygously floxed for both subunits, but these mice either lacked CreERT2 expression (GLAST$^{+/+}$) and were injected with tamoxifen (tam control) or expressed CreERT2 and received oil (oil control). We achieved an almost-complete loss of GluA1 and GluA4 expression in the molecular layer (ML) of dKO mice as assessed by confocal analysis (Fig. 1, B to I). We also determined a reduction of 85 and 50% of GluA1 and GluA4*pan* (*12*) mRNA expression, respectively, and ~70% of total GluA1/A4*L* (*12*) protein expression in cerebellar homogenates (fig. S1, A and B).

The loss of functional BG AMPARs was confirmed by whole-cell recordings and puff application of AMPA with D-aspartate to activate both AMPARs and glutamate transporters (Fig. 1J). BG cells of tam and oil controls exhibited similar transporter [DL-threo-β-benzyloxyaspartate (TBOA)–sensitive] and AMPAR [6-nitro-7-sulfamoylbenzo[f]quinoxaline-2,3-dione (NBQX)–sensitive] currents. However, in dKO mice, AMPAR currents were completely abolished (Fig. 1, J and K). Although in GLAST$^{CreERT2/+}$ cerebellar homogenates mRNA and protein levels were reduced, confocal analysis of GLAST immunolabeling revealed no overt differences (fig. S2), and BG cells of dKO and oil controls had comparable transporter currents to tam controls, although they are heterozygous for the GLAST locus (Fig. 1K). Thus, functional membrane expression of glutamate transporters was unaltered and should not influence any phenotype observed in dKO mice.

The gross cerebellar organization was unaffected when BG AMPARs were lost in the third postnatal week of cerebellar development (fig. S3). However, because Ca^{2+} signaling of BG AMPARs is important for synaptic transmission of PC synapses (*6*), we asked whether selective loss of BG AMPAR signaling influenced synaptic input to PCs. We analyzed parallel fiber (PF)–evoked PC currents (PF-EPSCs) in dKO mice and found an increase in amplitude, half-width, and decay time (Fig. 2, A and B). As expected, increase of half-width and decay time was more pronounced in dKO mice after blockade of AMPAR desensitization (fig. S4). These data point to an impaired clearance of synaptically released glutamate resulting from BG process retraction at PC spines (*6*). Indeed, light microscopic and ultrastructural inspection revealed that BG processes were, to a large extent, retracted from PC spines and lacked their characteristic complex morphology (Fig. 2E and fig. S5). Together with previous findings (*6*), these data emphasize the importance of glutamate and Ca^{2+}-mediated modulation of the cytoskeleton in perisynaptic astroglial processes (*13*). Moreover, we found a decrease in miniature EPSC frequency (Fig. 2, C and D) in PCs of dKO mice. Ultrastructural analysis of PF-PC synapse density confirmed a reduction 12 days after treatment (Fig. 2E and fig. S6). Additionally, dKO mice

[1]Department of Molecular Physiology, University of Saarland, Homburg, Germany. [2]Department of Neurogenetics, Max Planck Institute of Experimental Medicine, Göttingen, Germany. [3]Fachbereich Biologie, Technische Universität Kaiserslautern, Kaiserslautern, Germany. [4]Department of Neuroscience, Erasmus MC, Rotterdam, Netherlands. [5]Department of Physiology, Ludwig-Maximilians University, Munich, Germany. [6]Institute for Stem Cell Research, Helmholtz Center Munich, Neuherberg, Germany. [7]Department of Clinical Neurobiology at the German Cancer Research Center and the Medical Faculty of the Heidelberg University, Heidelberg, Germany. [8]Department of Molecular Neurobiology, Max Planck Institute of Medical Research, Heidelberg, Germany. [9]Department of Otolaryngology, University of Pittsburgh, Pittsburgh, PA, USA. [10]Netherlands Institute for Neuroscience, Royal Netherlands Academy of Arts and Sciences (KNAW), Amsterdam, Netherlands.

*These authors contributed equally to this work.
†Present address: Faculty of Life Sciences, University of Manchester, Manchester, UK.
‡Present address: Systems Neuroscience, Bernstein Focus for Neurotechnology and Johann-Friedrich-Blumenbach Institut für Zoologie und Anthropologie, Georg-August-Universität Göttingen, Germany.
§To whom correspondence should be addressed. E-mail: frank.kirchhoff@uks.eu (F.K.); c.dezeeuw@erasmusmc.nl (C.I.D.Z.)

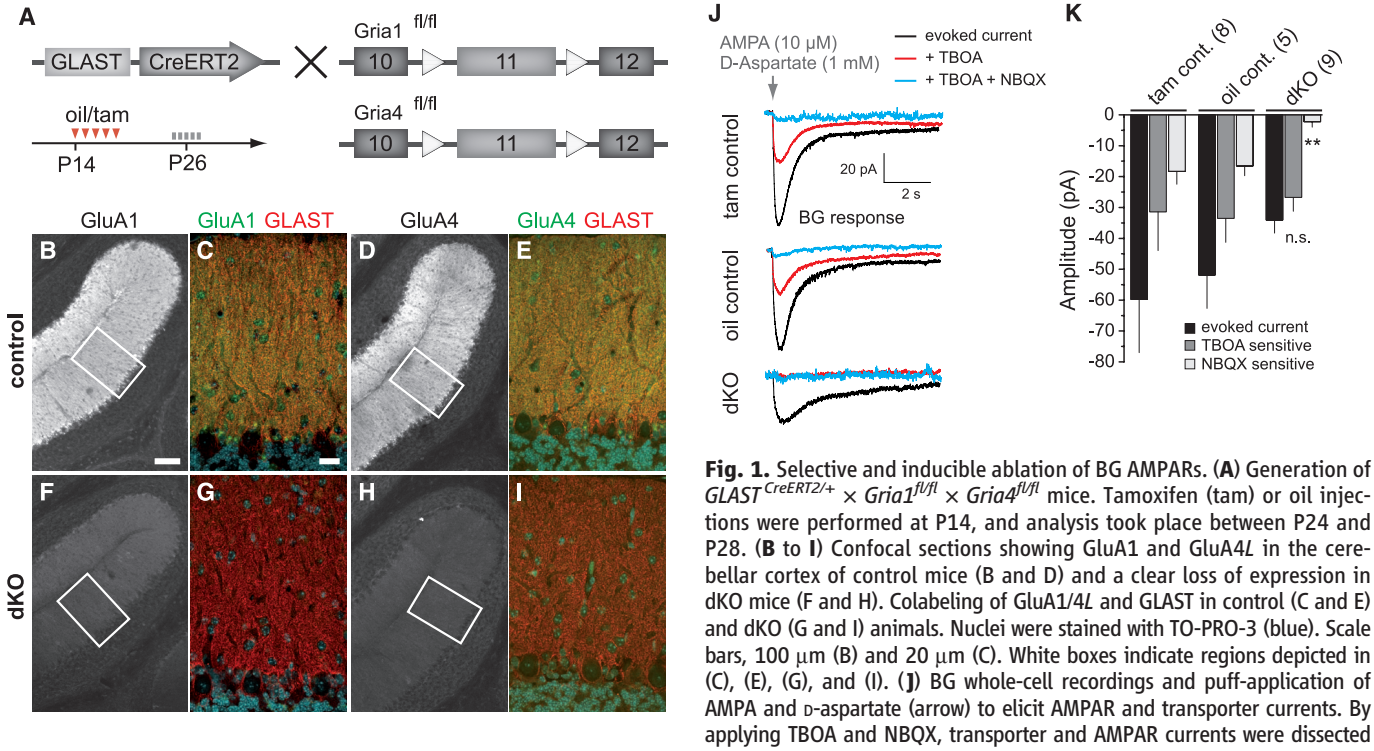

Fig. 1. Selective and inducible ablation of BG AMPARs. (**A**) Generation of *GLAST*$^{CreERT2/+}$ × *Gria1*$^{fl/fl}$ × *Gria4*$^{fl/fl}$ mice. Tamoxifen (tam) or oil injections were performed at P14, and analysis took place between P24 and P28. (**B** to **I**) Confocal sections showing GluA1 and GluA4*L* in the cerebellar cortex of control mice (B and D) and a clear loss of expression in dKO mice (F and H). Colabeling of GluA1/4*L* and GLAST in control (C and E) and dKO (G and I) animals. Nuclei were stained with TO-PRO-3 (blue). Scale bars, 100 μm (B) and 20 μm (C). White boxes indicate regions depicted in (C), (E), (G), and (I). (**J**) BG whole-cell recordings and puff-application of AMPA and D-aspartate (arrow) to elicit AMPAR and transporter currents. By applying TBOA and NBQX, transporter and AMPAR currents were dissected and quantified in (**K**). BG cells of dKO mice showed complete loss of AMPAR currents, whereas transporter currents remained unaltered compared with tam and oil controls. $^{**}P < 0.01$; ns, not significant.

showed reduced levels of vesicular glutamate transporter (VGlut1), a marker for PF terminals (Fig. 2F) (*14*). Yet, there were no signs of inflammation, activated microglia, or apoptosis (fig. S7). At 30 (instead of 12) days postinjection, PF-PC synapse density in dKO mice reached control levels (fig. S6A), whereas BG process retraction was still very obvious (fig. S6B). We conclude that during cerebellar development, PF-PC synapse formation is at least partially regulated by BG AMPAR signaling. Our results provide additional in vivo evidence to previous findings that astrocytes are involved in synapse formation (*15*, *16*). We could not, however, detect any differences in PF-PC synaptic plasticity such as paired pulse facilitation or long-term depression (figs. S8 and S9). We also did not observe an increase in climbing fiber terminals (fig. S10), but we cannot exclude a more subtle effect on elimination of multiple PC climbing fiber innervations (*6*).

At first glance, ablation of BG AMPARs during cerebellar development (at P14) did not cause any obvious ataxia. However, when dKO mice were challenged by running on a simple horizontal ladder, they revealed motor coordination deficits (fig. S11A). Unfortunately, the observed phenotype in young mice could have potentially been biased by side effects of the tamoxifen treatment, because it influenced body-weight gain compared with oil-treated animals (fig. S11B). Hence, we thoroughly analyzed cerebellar motor behavior in adult injected animals, because body weight of adult mice was unaffected by tamoxifen treatment.

To obtain a more robust gene expression–behavior relation, we quantified the time courses of tamoxifen-induced gene excision, mRNA degradation, and protein loss and correlated these with the accompanied structural and behavioral alterations. Recombination kinetics differed between the floxed *Gria1* and *Gria4* alleles: Maximal gene recombination for Gria1 was achieved 3 days after the first injection, whereas for Gria4 it required more than 7 days (fig. S12C). Similarly, mRNA and protein loss was faster for GluA1 (Fig. 3A and fig. S12D). For both subunits, complete loss of BG AMPAR expression was achieved 3 weeks after tamoxifen treatment (Fig. 3A and fig. S13), demonstrating a clear difference in turnover kinetics of BG AMPAR subunits in young and adult mice (fig. S14).

We next evaluated whether AMPAR inactivation in adults caused BG process retraction from PC spines. Three weeks after tamoxifen treatment, we could not observe any overt process retraction in dKO mice, although GluA1/A4 subunit expression was already completely lost (Fig. 3, B and D). However, 3 months after treatment, dKO mice displayed a significant reduction in BG appendage area and retraction from PC synapses (Fig. 3, C and D).

Does the loss of BG AMPAR signaling and subsequent retraction from PC synapses influence cerebellar function? We investigated the motor behavior of adult dKO mice at different periods after injections. We chose two cerebellum-related behavioral tasks, including locomotion conditioning on the Erasmus Ladder (Neurasmus BV, Rotterdam, Netherlands) (Fig. 4A) (*12*, *17*) and Pavlovian eyeblink conditioning (*18*, *19*), both of which allowed us to assess motor performance and motor learning in dKO mice during the same paradigm (Fig. 4 and figs. S15 and S16). First, we ruled out side effects of tamoxifen treatment on motor behavior by testing motor performance before and directly after injections (Fig. 4B). Performance was identical in both control groups as compared with inducible dKO mice (at that stage, there was no loss of AMPARs), indicating that the treatment itself did not affect motor performance. At 3 weeks postinjections, when loss of AMPARs was completed, we did not yet observe an overt difference in motor performance

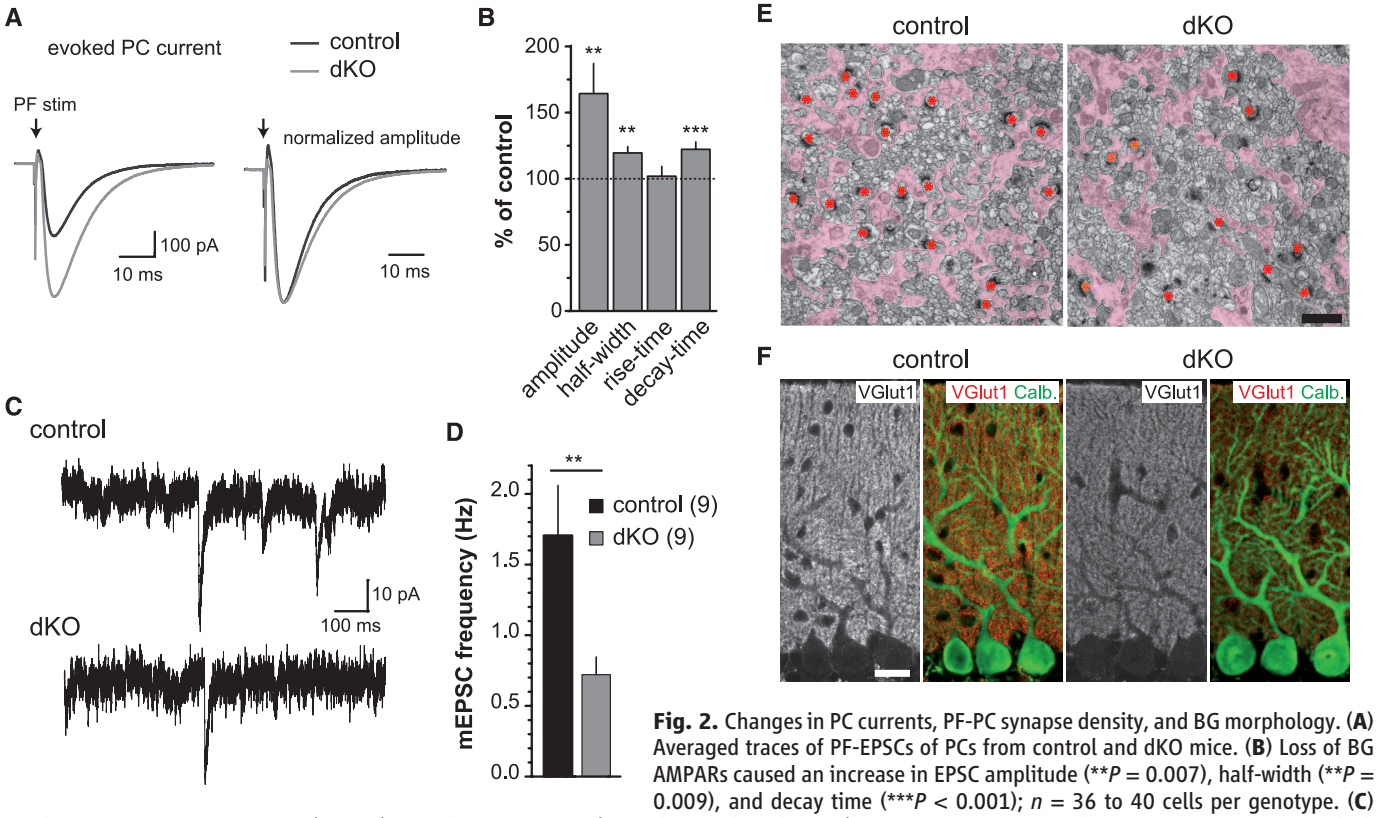

Fig. 2. Changes in PC currents, PF-PC synapse density, and BG morphology. (**A**) Averaged traces of PF-EPSCs of PCs from control and dKO mice. (**B**) Loss of BG AMPARs caused an increase in EPSC amplitude (**P = 0.007), half-width (**P = 0.009), and decay time (***P < 0.001); n = 36 to 40 cells per genotype. (**C**) Example traces of miniature EPSC (mEPSC) recordings from PCs (control, top; dKO, bottom) in 10 μM gabazine and 500 nM tetrodotoxin to block inhibitory input and action potential–evoked responses. (**D**) PCs from dKO mice showed reduced mEPSC frequency by 57.7 ± 7.3% (n = 9; **P = 0.009). (**E**) Ultrastructural analysis of PF-PC synapses in the upper third of the ML in control (left) and dKO (right) cells. BG processes are false-colored in pink, and synapses indicated with red asterisks. BG process complexity, synapse coverage, and synapse density were markedly reduced in dKO mice. Scale bar, 1 μm. (**F**) Confocal sections showing VGlut1 (for PF synapses) and calbindin (for PCs) in control (left) and dKO (right). VGlut1 expression was decreased by 36.3 ± 7.3% (n = 7 versus 8; P = 0.0003) in the ML of dKO mice. Scale bar, 20 μm.

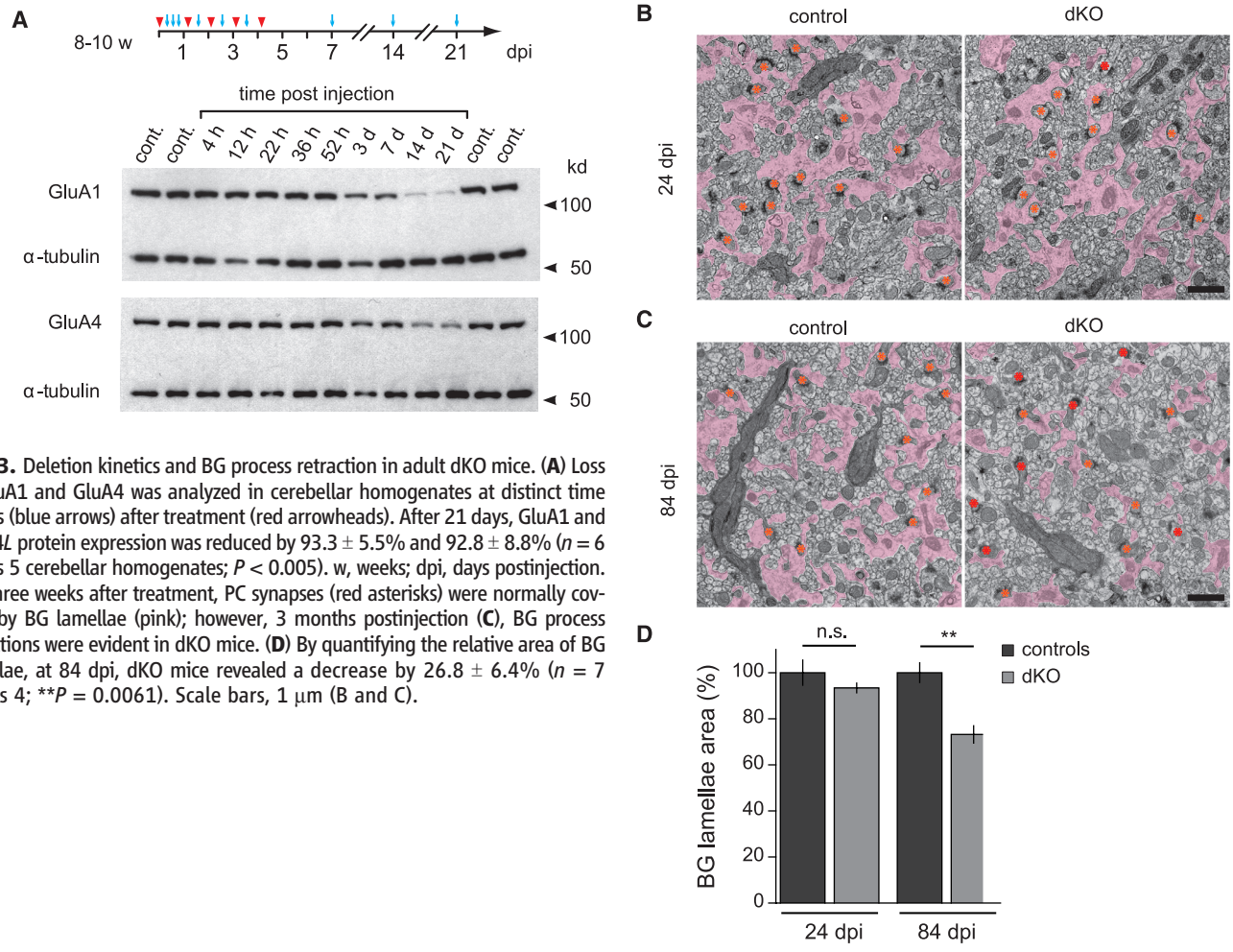

Fig. 3. Deletion kinetics and BG process retraction in adult dKO mice. (**A**) Loss of GluA1 and GluA4 was analyzed in cerebellar homogenates at distinct time points (blue arrows) after treatment (red arrowheads). After 21 days, GluA1 and GluA4*L* protein expression was reduced by 93.3 ± 5.5% and 92.8 ± 8.8% ($n = 6$ versus 5 cerebellar homogenates; $P < 0.005$). w, weeks; dpi, days postinjection. (**B**) Three weeks after treatment, PC synapses (red asterisks) were normally covered by BG lamellae (pink); however, 3 months postinjection (**C**), BG process retractions were evident in dKO mice. (**D**) By quantifying the relative area of BG lamellae, at 84 dpi, dKO mice revealed a decrease by 26.8 ± 6.4% ($n = 7$ versus 4; $^{**}P = 0.0061$). Scale bars, 1 μm (B and C).

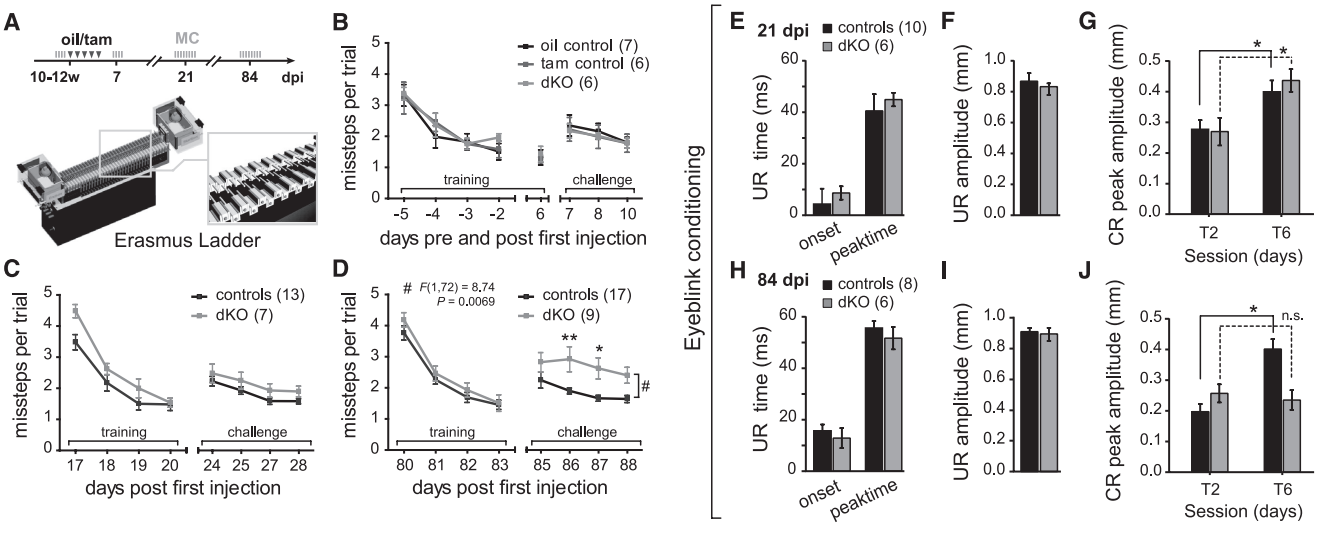

Fig. 4. Impaired fine motor coordination in mice lacking BG AMPARs. (**A**) At different time points before and/or after oil or tamoxifen treatment, motor coordination (MC) (i.e., average missteps per trial) was evaluated on the Erasmus Ladder (*12*, *17*). (**B**) Tamoxifen treatment had no side effects on motor behavior, as control groups and dKO mice performed equally well directly after treatment. (**C**) At 3 to 4 weeks postinjections, dKO mice showed no differences in motor performance and motor learning. (**D**) At 3 months after treatment, dKO mice performed well during training sessions, but revealed more missteps when challenged with an abruptly elevated ladder rung ($F_{1,72} = 8.74$, $P = 0.0069$, two-way analysis of variance with Bonferroni's posttest). (C and D) Tam and oil controls were pooled. (**E** to **J**) Analysis of eyeblink conditioning data at 3 weeks (E to G) and 3 months (H to J) after treatment. dKO mice and littermate controls showed normal reflexive eyelid closure (UR) in response to the corneal air puff (E, F and H, I). The increase in amplitude of the conditioned response (CR) after consecutive training sessions was identical in controls and dKO mice at 24 dpi (G); however, at 84 dpi, dKO mice failed to increase their CR amplitude ($P > 0.4$) compared with controls ($P < 0.05$) (J). Data are represented as ± SEM.

of dKO mice (Fig. 4C). dKO mice did not reveal BG process retractions at that stage (see above). However, 3 months after injections, when BG process retraction was evident, dKO mice displayed significant deficits in their motor performance when challenged on the Erasmus Ladder (Fig. 4D); they showed more missteps per trial. There were no signs of learning deficits, in that dKO mice improved their performance during the training sessions, similar to controls. When we subjected the animals at the same postinjection periods to the eyeblink conditioning paradigm, we observed that timing and amplitude of unconditioned responses (URs) of dKO mice (Fig. 4, E, F, H, and I), as well as rate of memory acquisition or extinction of conditioned responses, (figs. S15 and S16) were indistinguishable from controls. However, at 3 months posttreatment, the amplitudes of their conditioned responses (extent of eyelid closures) were significantly lower than those of controls after consecutive training sessions (Fig. 4J). Retraction of BG processes from PC synapses may impair timing of PC firing (with millisecond precision), which, in turn, would affect the output of cerebellar nuclei neurons and, thus, conditioned behavior (*20*, *21*).

We addressed the role of BG AMPARs on cerebellar function by generating conditional AMPAR mutants where both GluA1 and GluA4 subunits were efficiently ablated in young and adult mice. We revealed that AMPAR signaling of BG cells contributes to the structural and functional integrity of the cerebellar network. Our results provide in vivo evidence that BG AMPARs play an important role in the fine-tuning of neuronal processing, which is crucial for a fast and precise control of complex motor behaviors.

References and Notes

1. A. Volterra, J. Meldolesi, *Nat. Rev. Neurosci.* **6**, 626 (2005).
2. A. Verkhratsky, F. Kirchhoff, *J. Anat.* **210**, 651 (2007).
3. G. Perea, M. Navarrete, A. Araque, *Trends Neurosci.* **32**, 421 (2009).
4. K. Matsui, C. E. Jahr, M. E. Rubio, *J. Neurosci.* **25**, 7538 (2005).
5. J. Grosche *et al.*, *Nat. Neurosci.* **2**, 139 (1999).
6. M. Iino *et al.*, *Science* **292**, 926 (2001).
7. T. Mori *et al.*, *Glia* **54**, 21 (2006).
8. D. Zamanillo *et al.*, *Science* **284**, 1805 (1999).
9. E. C. Fuchs *et al.*, *Neuron* **53**, 591 (2007).
10. T. Müller, T. Möller, T. Berger, J. Schnitzer, H. Kettenmann, *Science* **256**, 1563 (1992).
11. N. Burnashev *et al.*, *Science* **256**, 1566 (1992).
12. For more details, see supplementary materials on *Science* Online.
13. M. Lavialle *et al.*, *Proc. Natl. Acad. Sci. U.S.A.* **108**, 12915 (2011).
14. H. Hirai *et al.*, *Nat. Neurosci.* **8**, 1534 (2005).
15. E. M. Ullian, S. K. Sapperstein, K. S. Christopherson, B. A. Barres, *Science* **291**, 657 (2001).
16. K. S. Christopherson *et al.*, *Cell* **120**, 421 (2005).
17. R. S. Van Der Giessen *et al.*, *Neuron* **58**, 599 (2008).
18. D. A. McCormick, R. F. Thompson, *Science* **223**, 296 (1984).
19. S. K. Koekkoek *et al.*, *Science* **301**, 1736 (2003).
20. C. I. De Zeeuw *et al.*, *Nat. Rev. Neurosci.* **12**, 327 (2011).
21. A. L. Person, I. M. Raman, *Nature* **481**, 502 (2012).

Acknowledgments: We thank K.-A. Nave for continuous support, S. Rudolph and P. G. Hirrlinger for early contributions, T. Ruhwedel and F. Rhode for technical assistance, and D. Rhode and C. Casper for animal husbandry. This work was supported by the Max-Planck Society (INSERM-AMIGO, F.K.); Deutsche Forschungsgemeinschaft (DFG)–Research Center Molecular Physiology of the Brain (F.K.); DFG-SPP 1172 (F.K. and J.W.D.); DFG-SFB870 (M.G.); DFG-SFB894 (F.K.); DFG-Transregio TRR43 (F.K.); European Union (EU)–FP7-202167 NeuroGLIA (F.K.) and FP7-ITN-237956 EdU-Glia (F.K.); RO1-DC006881 (M.E.R.); the Research Initiative in Membrane Biology University of Kaiserslautern (J.W.D.); the Dutch Organization for Medical Sciences (C.I.D.Z.); Life Sciences (C.I.D.Z.); Fund for Economic Structure Reinforcement (NeuroBasic; C.I.D.Z.); Prinses Beatrix Fonds (C.I.D.Z.); and the EU ERCadvanced, CEREBNET, and C7 programs (C.I.D.Z.).

Supplementary Materials

www.sciencemag.org/cgi/content/full/science.1221140/DC1
Materials and Methods
Supplementary Text
Figs. S1 to S16
References (*22*–*35*)

27 February 2012; accepted 14 June 2012
Published online 5 July 2012;
10.1126/science.1221140

The Pulvinar Regulates Information Transmission Between Cortical Areas Based on Attention Demands

Yuri B. Saalmann,[1,2]* Mark A. Pinsk,[1,2]† Liang Wang,[1,2]† Xin Li,[1,2] Sabine Kastner[1,2]

Selective attention mechanisms route behaviorally relevant information through large-scale cortical networks. Although evidence suggests that populations of cortical neurons synchronize their activity to preferentially transmit information about attentional priorities, it is unclear how cortical synchrony across a network is accomplished. Based on its anatomical connectivity with the cortex, we hypothesized that the pulvinar, a thalamic nucleus, regulates cortical synchrony. We mapped pulvino-cortical networks within the visual system, using diffusion tensor imaging, and simultaneously recorded spikes and field potentials from these interconnected network sites in monkeys performing a visuospatial attention task. The pulvinar synchronized activity between interconnected cortical areas according to attentional allocation, suggesting a critical role for the thalamus not only in attentional selection but more generally in regulating information transmission across the visual cortex.

The limited capacity of the visual system does not permit simultaneous processing of all information from our cluttered environment in detail. Selective attention helps overcome this limitation by preferentially routing behaviorally relevant information across the visual system. Simultaneous neural recordings from two cortical areas have suggested that this selective routing depends on the degree of synchrony between neuronal groups in each cortical area (*1*–*4*). However, it is unclear how different cortical areas synchronize their activity. Although direct interaction between two cortical areas may give rise to their synchrony, an alternative possibility is that a third area, connected to both of them, mediates cortical synchronization.

Higher-order thalamic nuclei, such as the pulvinar, predominantly receive input from the cortex rather than the periphery, and their output strongly influences cortical activity in in vitro experiments (*5*). Because directly connected cortical areas are also indirectly connected via the pulvinar (fig. S1), the pulvinar is ideally positioned to synchronize activity across the visual cortex (*6*–*8*). However, little is known about the functional role of these cortico-pulvino-cortical loops. Selective attention modulates the magnitude of response of macaque pulvinar neurons (*9*, *10*), and both humans and macaques with pulvinar lesions commonly have attentional deficits (*11*, *12*). We therefore hypothesized that the pulvinar increases synchrony between sequential processing stages across the visual cortex during selective attention.

Information transmitted along the ventral visual cortical pathway is sequentially processed in interconnected areas V4 and the temporo-occipital area (TEO). We simultaneously recorded neural activity in macaques in the pulvinar, V4, and TEO during 51 recording sessions (*13*). Spike trains and local field potentials (LFPs) were recorded in each area from neurons with overlapping receptive fields (RFs). Monkeys performed a variant of the Eriksen flanker task, in which a spatial cue signals the location of a subsequent target flanked by distracter stimuli (target detection >80% accuracy overall; Fig. 1A). Because directly connected cortical areas such as V4 and TEO only connect with restricted but overlapping zones in the pulvinar (*8*, *14*), we used diffusion tensor imaging (DTI) to ensure that electrodes targeted interconnected pulvino-cortical sites.

We performed probabilistic tractography on DTI data for each monkey to map probable

[1]Princeton Neuroscience Institute, Princeton University, Princeton, NJ 08544, USA. [2]Department of Psychology, Princeton University, Princeton, NJ 08544, USA.

*To whom correspondence should be addressed. E-mail: saalmann@princeton.edu
†These authors contributed equally to this work.